THE JOURNAL OF PHYSICAL CHEMISTRY Letters

pubs.acs.org/JPCL

Confocal Fluorescence Microscopy of the Morphology and Composition of Interstitial Fluids in Freezing Electrolyte Solutions

Jie Cheng, Cherrie Soetjipto, Michael R. Hoffmann, and A. J. Colussi*

W. M. Keck Laboratories, California Institute of Technology, Pasadena, California 91125

ABSTRACT Ice rheology, the integrity of polar ice core records, and ice−atmosphere interactions are among the phenomena controlled by the morphology and composition of interstitial fluids threading polycrystalline ice. Herein, we investigate how ionic impurities affect such features via time-resolved confocal fluorescence microscopy of freezing electrolyte solutions doped with a pH probe. We find that the 10 μM probe accumulates into 12 μm thick glassy channels in frozen water, but it is incorporated into randomly distributed < 1 μm diameter inclusions in freezing 1 mM NaCl. We infer that morphology is largely determined by the dynamic instabilities generated upon advancing ice by the rejected solute, rather than by thermodynamics. The protracted alkalinization of the fluid inclusions reveals that the excess negative charge generated by the preferential incorporation of Cl^- over Na^+ in ice is neutralized by the seepage of the OH^- slowly produced via $H_2O \rightarrow H^+ + OH^-$ thermal dissociation.

SECTION Atmospheric, Environmental and Green Chemistry

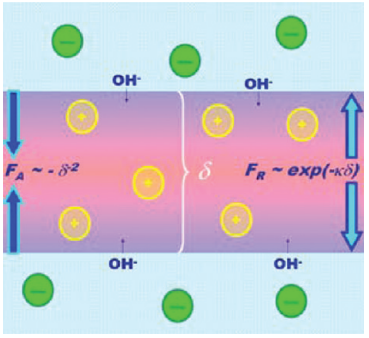

Most technologically important materials are polycrystalline aggregates held together by disordered phases.[1] The rheology of glacial ice,[2−6] the tensile strength of steel, and the conductivity of superconductors[7] are affected by the composition and geometry of grain boundaries. Grains arise because advancing solid/melt fronts are destabilized and bifurcate under the perturbations induced by the local release of latent heat and the rejection of impurities upon solidification.[8,9] These inhomogeneities persist for dynamic rather than thermodynamic reasons. The global lowest free energy configuration in the case of water is an ice single crystal covered by unfrozen fluid containing the rejected impurities.[10−14]

Ice is extremely intolerant to impurities, but interstitial fluids are not concentrates of the starting solutions.[15−19] Some species, such as NH_4^+ and F^-, which are isoelectronic and nearly isomorphous with H_2O and OH^-, respectively, are marginally (~0.01 %) but preferentially incorporated over other ions into the ice matrix. This phenomenon generates charge imbalances between the solid and liquid phases,[20] which ultimately relax via migration of the intrinsic H^+/HO^- ice carriers.[15,21,22] The selective incorporation of cations into the ice lattice should therefore lead to the acidification of the unfrozen portion, and vice versa. The acidity of interstitial fluids determines whether weak volatile acids or bases are exchanged between ice and the gas phase or whether reactions between dopants are inhibited or catalyzed upon freezing.[23−27] Chemical[28,29] and biological activity[30] in snow, ice cores, and permafrost actually occurs in intergranular microfluids containing the solutes and nutrients rejected by the solid matrix.

Premelted films at the air/ice interface have been extensively investigated, both theoretically and experimentally.[31−36] Much less information is available on interstitial fluids.[3,4,37−39] The experimental study of optically transparent polycrystalline ice seems ideally suited to advance our understanding of the nature of grain boundaries. Herein, we report preliminary results of the first time-resolved confocal fluorescence microscopy study of freezing aqueous electrolyte solutions[4,40−42] and their subsequent thawing.

Figure 1 shows that under a preset -10.0 K min^{-1} ramp, the sample temperature T_s actually fell to ~268 K at -7.9 K min^{-1}. At this point freezing began, raising T_s to 273 K. T_s remained at ~273 K during freezing, before falling to 265 K for the rest of stage 2. The time elapsed between the onset and completion of freezing was ~125 s.

Different cooling ramps affected the ice front velocity, v, rather than T_s. The ice front typically moved radially inward toward the axis of the cylindrical sample at $v \approx 5$ μm s^{-1}. In this process, the fluorescent probe is rejected into liquid inclusions whose morphology critically depends on the absence or presence of other electrolytes (Figure 2a−c). C-SNARF-1 in Milli-Q water or in μM electrolyte solutions accumulates into liquid channels arranged in a cellular network of well-developed $\delta = (12 \pm 2)$ μm thick veins within very pure (deep blue) ice (Figure 2a). Figure 3a−d shows in more detail the fluorescence intensity and pH (x, y)-distributions during the

Received Date: October 4, 2009
Accepted Date: December 3, 2009
Published on Web Date: December 10, 2009

DOI: 10.1021/jz9000888 | *J. Phys. Chem. Lett.* **2010**, *1*, 374–378

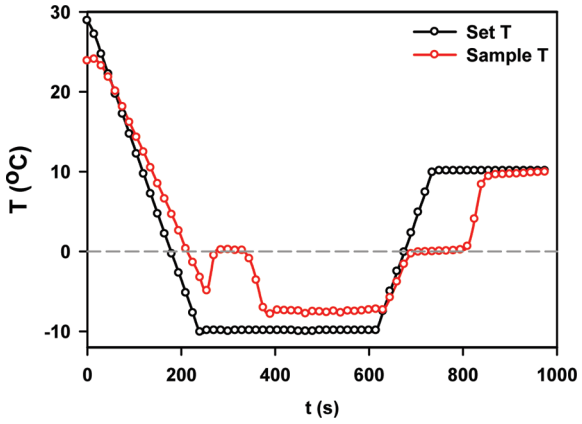

Figure 1. Black: programmed temperature. Red: actual sample temperature.

freezing and thawing of a ([C-SNARF-1] = 10 μM, [NaCl] = 0.1 mM) solution.

Figure 3a shows that the probe is evenly distributed in the sample solution at pH 6.4 over the entire field of view prior to freezing. About 10 s after the onset of freezing, the C-SNARF-1 rejected by solid accumulates within a ~30 μm half-width diffuse band centered ~20 μm ahead of the ice front (Figure 3b). Figure 3b and c shows that the pH increases from 6.4 to 7.2 at the band center on this time scale and up to 7.0 in the liquid inclusions farther away. The pH, however, rises to 8.4 upon thawing samples that have been frozen for 5 min. This slow response is seemingly associated with the seepage of OH^- into liquid inclusions at rates consistent with its production via the thermal dissociation of water, $H_2O \rightarrow H^+ + OH^-$, with a rate constant $k_f = K_w k_b \approx 10^{-14}$ M $\times$ 10^{11} M^{-1} $s^{-1} \approx 10^{-3}$ s^{-1}.[17,18,43] The pH reverts to its initial 6.4 value after the thawed sample homogeneizes itself. A similar freeze-and-thaw cycle for 0.05 mM CH_3COONH_4 solutions initially at pH 7.9 leads to a more acidic melt at pH 6.8, as expected from the preferential incorporation of NH_4^+ in the ice lattice (Figure S1, Supporting Information, SI).[17,43] Note that the concentration of aqueous NaCl solutions in equilibrium with pure ice at 268 K is 2.27 *m*.[44] The volume fraction of interstitial fluids, VF_{IF} = 1 m*m*/2.27 *m* = 0.044 %, in a frozen 1 mM (~1 m*m*) NaCl solution in equilibrium at 268 K corresponds to an interstitial volume V_{IF} = 13.2 nL in our 30 μL samples. This volume is equivalent to $N > 2.5 \times 10^7$ quasi-spherical inclusions of < 1 μm diameter. Since the solubility of C-SNARF-1 is certainly exceeded in frozen water at 268 K, the fluorescence emissions observed in Figure 2a represent evidence that the probe has not crystallized but remains dispersed in a glassy medium.

The cellular structures evident in frozen doped water are typical of those produced by spontaneous dynamic instabilities in systems far from equilibrium (Figure 2a).[45] The brine inclusions from which the probe emits in frozen 1 mM NaCl or $(NH_4)_2SO_4$ solutions (Figure 2b, c) represent an alternative outcome of freezing from otherwise identical initial conditions. Upon freezing, latent heat is released while rejected solutes concentrate in the liquid at the ice front.[46−48] The consequences of these perturbations depend on the competition between ice front velocities with thermal and mass

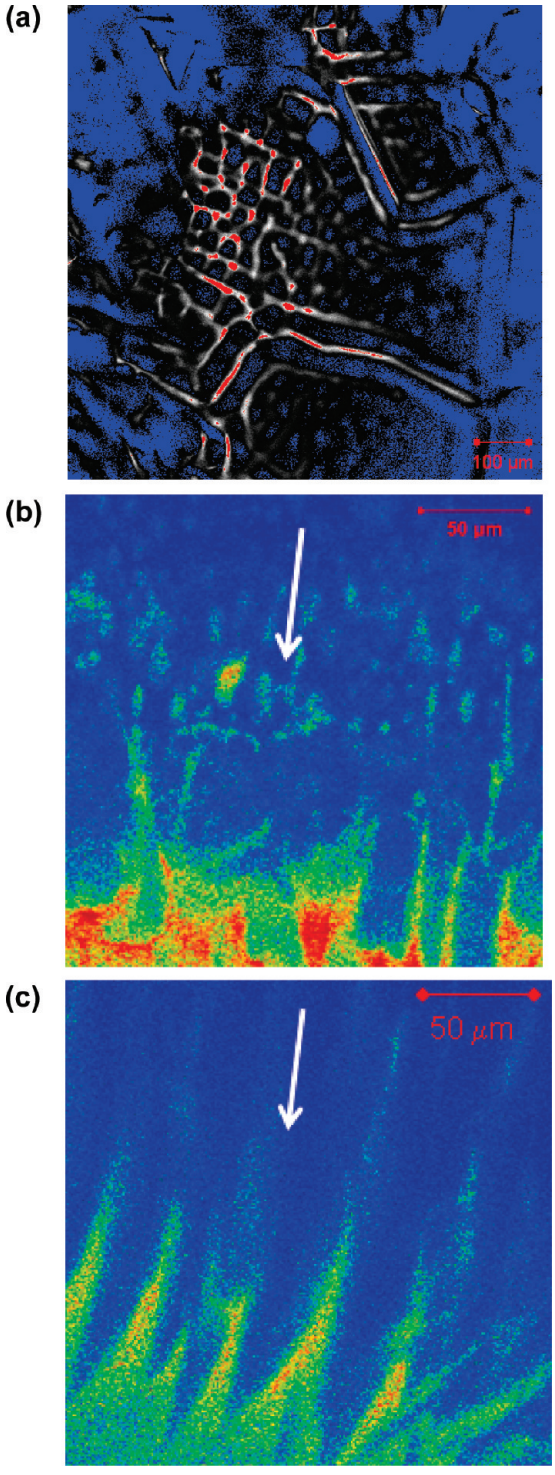

Figure 2. Images of frozen 10 μM C-SNARF-1 solutions in (a) deionized water, (b) 1 mM NaCl, and (c) 1 mM $(NH_4)_2SO_4$. Fluorescence intensities are on a rainbow scale (blue: low intensity). Frame sizes: (a) 900 μm $\times$ 900 μm; (b) and (c) 225 μm $\times$ 225 μm.

diffusion rates, respectively. Thermal and concentration fluctuations eventually trigger the formation of ice protrusions at planar fronts, which amplify themselves because the thermal conductivity of ice is ~3.5 times larger than that of water.

DOI: 10.1021/jz9000888 | *J. Phys. Chem. Lett.* **2010**, *1*, 374–378

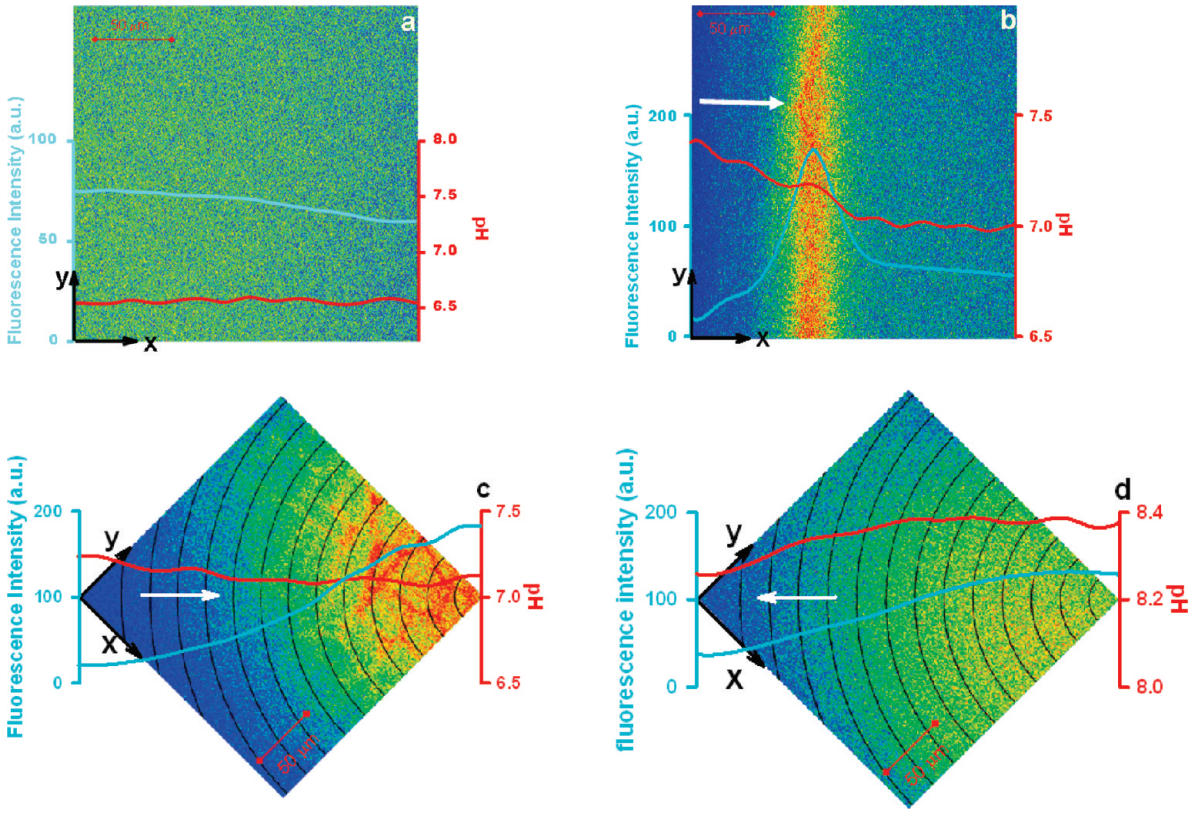

Figure 3. Fluorescence intensities (cyan line) and pH values (red line) in an aqueous 10 μM C-SNARF-1/0.1 mM NaCl solution (a) before freezing, (b) 9.8 s after freezing began, (c) 52.4 s after freezing began, and (d) 20 s after thawing began. Fluorescence intensity curves represent integrated intensities of isosbestic point (λ_{iso} = 615 nm) emissions; $\langle F(x)\rangle = [\int F(x,y)dy]/\int dy$ (Figure 3a, b), or $\langle F(\rho)\rangle = [\int F(\rho,\varphi)d\varphi]/\int d\varphi$ (Figure 3c, d). The pH values are based on integrated intensity ratios, $R = \langle F(581\text{ nm})\rangle/\langle F(635\text{ nm})\rangle$. Frame size is 225 μm × 225 μm throughout. White arrows indicate the direction of freezing (b, c) or thawing (d).

Depending on the conditions, these columnar arrays become themselves unstable toward perturbations normal to the advancing dendrites. Ice bridges may develop across dendrites that will encapsulate the liquid into spheroidal inclusions.[49] This process is akin to the breakup of liquid jets into droplets via Rayleigh instabilities. Thermodynamics dictates that these inclusions should ultimately coalesce to minimize the overall surface-to-volume ratio. The processes by which equilibrium is reached may, however, be immeasurably slow. It is apparent that any explanation for the dissimilar outcomes of freezing water and 1 mM electrolytes on the time scale of present experiments cannot be exclusively based on thermodynamics (see Appendix S1, SI). The complex dynamics of freezing in a supersaturated solution may be affected, but it is not determined by the short-range dispersive and long-range shielded Coulombic forces that would arise among approaching ice grains.[50] Recent molecular dynamics calculations actually suggest that the role of impurities is to perturb the cooperativity of molecular motions during freezing[1,51] and that interstitial fluids at grain boundaries resemble glassy materials whose properties and morphology are very sensitive to impurities.[52−57]

Summing up, we have shown that confocal fluorescence microscopy of freezing aqueous solutions is an incisive experimental tool for investigating the development and properties of interstitial fluids. A more comprehensive study of solute concentration, undercooling, and annealing effects on the morphology of grain boundaries is underway.

Scheme 1. C-SNARF-1, 4-(10-(Dimethylamino)-3-oxo-3H-benzo-[*c*]xanthen-7-yl)isophthalic Acid

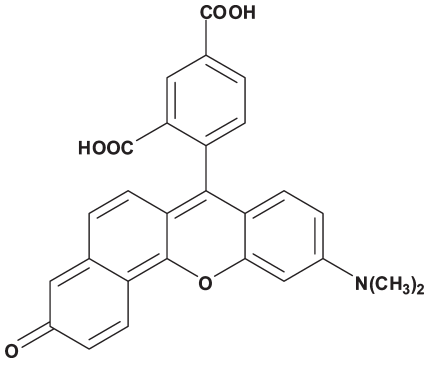

Experimental Methods

The dual-emission fluorescence pH indicator C-SNARF-1 (Scheme 1) was used in our experiments.[58,59] Fluorescence spectra of C-SNARF-1 excited at λ_{exc} = 488 or 514 nm display two maxima at λ_1 = 581 nm and λ_2 = 635 nm (isosbestic emission point at λ_{iso} = 615 nm) whose relative intensities

DOI: 10.1021/jz9000888 | J. Phys. Chem. Lett. 2010, 1, 374–378

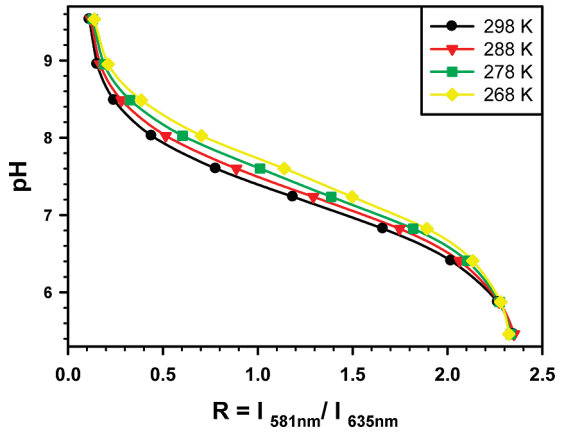

Figure 4. C-SNARF-1 fluorescence emission ratios, $R = I(581\ nm)/I(635\ nm)$, versus pH from (1.0 μM C-SNARF-1/50 mM phosphate buffer) solutions at various temperatures.

sensitively depend on pH (Figure 4 and Figure S2, SI). Temporally and spatially resolved fluorescence emission spectra from test solution samples (30 μL; 6 mm diameter, 1 mm deep) were obtained with a confocal laser scanning microscope equipped with a programmable cryostage set to (1) cool at $-10\ K\ min^{-1}$ from 298 to 268 K, (2) hold at 268 K for 5 min after freezing completion, and (3) warm at $10\ K\ min^{-1}$ to 298 K. Actual sample temperatures, T_s, were determined with a fast-response thermocouple dipping into the test solution. Further details are provided in the SI.

SUPPORTING INFORMATION AVAILABLE Additional data and experimental details. This material is available free of charge via the Internet at http://pubs.acs.org.

AUTHOR INFORMATION

Corresponding Author:

*To whom correspondence should be addressed. Phone: 01-626-395-4402. Fax: 01-626-395-2940. E-mail: ajcoluss@caltech.edu.

ACKNOWLEDGMENT This project was financially supported by the National Science Foundation (ATM-0534990). C.S. thanks a James J. Morgan SURF Fellowship.

REFERENCES

(1) Zhang, H.; Srolovitz, D. J.; Douglas, J. F.; Warren, J. A. Grain Boundaries Exhibit the Dynamics of Glass-Forming Liquids. *Proc. Natl. Acad. Sci. U.S.A.* **2009,** *106*, 7735–7740.
(2) Rempel, A. W.; Wettlaufer, J. S. Segregation, Transport, And Interaction of Climate Proxies in Polycrystalline Ice. *Can. J. Phys.* **2003,** *81*, 89–97.
(3) Barnes, P. R. F.; Wolff, E. W. Distribution of Soluble Impurities in Cold Glacial Ice. *J. Glaciol.* **2004,** *50*, 311–324.
(4) Baker, I.; Iliescu, D.; Obbard, R.; Chang, H.; Bostick, B.; Daghlian, C. P. Microstructural Characterization of Ice Cores. *Ann. Glaciol.* **2005,** *42*, 441–444.
(5) Duval, P.; Arnaud, L.; Brissaud, O.; Montagnat, M.; de la Chapelle, S. Deformation and Recrystallization Processes of Ice from Polar Ice Sheets. *Ann. Glaciol.* **2000,** *30*, 83–87.
(6) Cullen, D.; Baker, I. The Chemistry of Grain Boundaries in Greenland Ice. *J. Glaciol.* **2000,** *46*, 703–706.
(7) Rettenmayr, M. Melting and Remelting Phenomena. *Int. Mater. Rev.* **2009,** *54*, 1–17.
(8) Nagashima, K.; Furukawa, Y. Solute Distribution in Front of an Ice/Water Interface during Directional Growth of Ice Crystals and Its Relationship to Interfacial Patterns. *J. Phys. Chem. B* **1997,** *101*, 6174–6176.
(9) Wettlaufer, J. S. Directional Solidification of Salt-Water. Deep and Shallow Cells. *Europhys. Lett.* **1992,** *19*, 337–342.
(10) Blackford, J. R. Sintering and Microstructure of Ice: A Review. *J. Phys. D: Appl. Phys.* **2007,** *40*, R355–R385.
(11) Durham, W. B.; McKinnon, W. B.; Stern, L. A. Cold Compaction of Water Ice *Geophys. Res. Lett.* 2005, *32*, doi: L18202 10.1029/2005gl023484.
(12) Chaudhary, V.; Mathur, P. Composite avalanche Control Scheme Developed for the Lower Himalayan Zone: A Case History. *Cold Reg. Sci. Technol.* **2004,** *39*, 243–255.
(13) Song, C.; Wang, P.; Makse, H. A. A Phase Diagram for Jammed Matter. *Nature* **2008,** *453*, 629–632.
(14) Torquato, S.; Stillinger, F. H. toward the Jamming Threshold of Sphere Packings: Tunneled Crystals *J. Appl. Phys.* 2007, *102*, doi: 09351110.1063/1.2802184
(15) Workman, E. J.; Reynolds, S. E. Electrical Phenomena Occurring during the Freezing of Dilute Aqueous Solutions and Their Possible Relationship to Thunderstorm Electricity. *Phys. Rev.* **1950,** *78*, 254–259.
(16) Killawee, J. A.; Fairchild, I. J.; Tison, J. L.; Janssens, L.; Lorrain, R. Segregation of Solutes and Gases in Experimental Freezing of Dilute Solutions: Implications for Natural Glacial Systems. *Geochim. Cosmochim. Acta* **1998,** *62*, 3637–3655.
(17) Robinson, C.; Boxe, C. S.; Guzmán, M. I.; Colussi, A. J.; Hoffmann, M. R. Acidity of Frozen Electrolyte Solutions. *J. Phys. Chem. B* **2006,** *110*, 7613–7616.
(18) Bronshteyn, V. L.; Chernov, A. A. Freezing Potentials Arising on Solidification of Dilute Aqueous-Solutions of Electrolytes. *J. Cryst. Growth* **1991,** *112*, 129–145.
(19) Heger, D.; Klanova, J.; Klan, P. Enhanced Protonation of Cresol Red in Acidic Aqueous Solutions Caused by Freezing. *J. Phys. Chem. B* **2006,** *110*, 1277–1287.
(20) Wilson, P. W.; Haymet, A. D. J. Workman—Reynolds Freezing Potential Measurements between Ice and Dilute Salt Solutions for Single Ice Crystal Faces. *J. Phys. Chem. B* **2008,** *112*, 11750–11755.
(21) Cobb, A. W.; Gross, G. W. Interfacial Electrical Effects Observed during Freezing of Dilute Electrolytes in Water. *J. Electrochem. Soc.* **1969,** *116*, 796–803.
(22) Gross, G. W.; Wong, P. M.; Humes, K. Concentration Dependent Solute Redistribution at Ice—Water Phase Boundary. 3. Spontaneous Convection — Chloride Solutions. *J. Chem. Phys.* **1977,** *67*, 5264–5274.
(23) O'Driscoll, P.; Minogue, N.; Takenaka, N.; Sodeau, J. Release of Nitric Oxide and Iodine to the Atmosphere from the Freezing of Sea-Salt Aerosol Components. *J. Phys. Chem. A* **2008,** *112*, 1677–1682.
(24) Sato, K.; Takenaka, N.; Bandow, H.; Maeda, Y. Evaporation Loss of Dissolved Volatile Substances from Ice Surfaces. *J. Phys. Chem. A* **2008,** *112*, 7600–7607.
(25) Takenaka, N.; Bandow, H. Chemical Kinetics of Reactions in the Unfrozen Solution of Ice. *J. Phys. Chem. A* **2007,** *111*, 8780–8786.
(26) Finnegan, W. G.; Pitter, R. L.; Hinsvark, B. A. Redox Reactions in Growing Single Ice Crystals: A Mechanistic Interpretation of Experimental Results. *J. Colloid Interface Sci.* **2001,** *242*, 373–377.

DOI: 10.1021/jz9000888 | *J. Phys. Chem. Lett.* **2010,** *1*, 374–378

(27) Betterton, E. A.; Anderson, D. J. Autoxidation of N(III), S(IV), and Other Species in Frozen Solution — A Possible Pathway for Enhanced Chemical Transformation in Freezing Systems. *J. Atmos. Chem.* **2001,** *40*, 171–189.
(28) Boxe, C. S.; Colussi, A. J.; Hoffmann, M. R.; Perez, I. M.; Murphy, J. G.; Cohen, R. C. Kinetics of NO and NO_2 Evolution from Illuminated Frozen Nitrate Solutions. *J. Phys. Chem. A* **2006,** *110*, 3578–3583.
(29) Dubowski, Y.; Colussi, A. J.; Boxe, C.; Hoffmann, M. R. Monotonic Increase of Nitrite Yields in the Photolysis of Nitrate in Ice and Water Between 238 and 294 K. *J. Phys. Chem. A* **2002,** *106*, 6967–6971.
(30) Price, P. B.; Rohde, R. A.; Bay, R. C. Fluxes of Microbes, Organic Aerosols, Dust, Sea-Salt Na Ions, Non-Sea-Salt Ca Ions, and Methanesulfonate onto Greenland and Antarctic Ice. *Biogeosciences* **2009,** *6*, 479–486.
(31) Dash, J. G.; Rempel, A. W.; Wettlaufer, J. S. The Physics of Premelted Ice and Its Geophysical Consequences. *Rev. Mod. Phys.* **2006,** *78*, 695–741.
(32) Wettlaufer, J. S.; Worster, M. G. Premelting Dynamics. *Ann. Rev. Fluid Mech.* **2006,** *38*, 427–452.
(33) Sadtchenko, V.; Ewing, G. E. Interfacial Melting of Thin Ice Films: An Infrared Study. *J. Chem. Phys.* **2002,** *116*, 4686–4697.
(34) Wei, X.; PB, M.; C, Z.; Shen, Y. R. Sum-Frequency Spectroscopic Studies of Ice Interfaces. *Phys. Rev. B* **2002,** *66*, 085401.
(35) Doppenschmidt, A.; Butt, H.-J. Measuring the Thickness of the Liquid-Like Layer on Ice Surfaces with Atomic Force Microscopy. *Langmuir* **2000,** *16*, 6709–6714.
(36) Goertz, M. P.; Zhu, X. Y.; Houston, J. E. Exploring the Liquid-Like Layer on the Ice Surface. *Langmuir* **2009,** *25*, 6905–6908.
(37) Nye, J. F. The Geometry of Water Veins and Nodes in Polycrystalline Ice. *J. Glaciol.* **1989,** *35*, 17–22.
(38) Barnes, P. R. F.; Wolff, E. W.; Mallard, D. C.; Mader, H. M. SEM Studies of the Morphology and Chemistry of Polar Ice. *Microsc. Res. Technol.* **2003,** *62*, 62–69.
(39) Rempel, A. W.; Waddington, E. D.; Wettlaufer, J. S.; Worster, M. G. Possible Displacement of the Climate Signal in Ancient Ice by Premelting and Anomalous Diffusion. *Nature* **2001,** *411*, 568–571.
(40) Zepeda, S.; Yokoyama, E.; Uda, Y.; Katagiri, C.; Furukawa, Y. In Situ Observation of Antifreeze Glycoprotein Kinetics at the Ice Interface Reveals a Two-Step Reversible Adsorption Mechanism. *Cryst. Growth Des.* **2008,** *8*, 3666–3672.
(41) Forster, T. Progression of Freezing and Cooling Curves during Dendritic Freezing Measured by Fluorescence Labels. *Cryo-Letters* **1986,** *7*, 87–94.
(42) Menger, F. M.; Galloway, A. L.; Chlebowski, M. E.; Apkarian, R. P. Ultrastructure in Frozen/Etched Saline Solutions: On the Internal Cleansing of Ice. *J. Am. Chem. Soc.* **2004,** *126*, 5987–5989.
(43) Takenaka, N.; Ueda, A.; Daimon, T.; Bandow, H.; Dohmaru, T.; Maeda, Y. Acceleration Mechanism of Chemical Reaction by Freezing: The Reaction of Nitrous Acid with Dissolved Oxygen. *J. Phys. Chem.* **1996,** *100*, 13874–13884.
(44) Potter, R. W.; Clynne, M. A.; Brown, D. L. Freezing-Point Depression of Aqueous Sodium-Chloride Solutions. *Econom. Geol.* **1978,** *73*, 284–285.
(45) Schliecker, G. Structure and Dynamics of Cellular Systems. *Adv. Phys.* **2002,** *51*, 1319–1378.
(46) Tiller, W. A. *The Science of Crystallization: Macroscopic Phenomena and Defect Generation*; Cambridge University Press: Cambridge, U.K., 1991.
(47) Shimada, W.; Furukawa, Y. Pattern Formation of Ice Crystals during Free Growth in Supercooled Water. *J. Phys. Chem. B* **1997,** *101*, 6171–6173.
(48) Tison, J. L.; Verbeke, V. Chlorinity/Salinity Distribution Patterns in Experimental Granular Sea Ice. *Ann. Glaciol* **2001,** *33*, 13–20.
(49) Maeda, N.; Israelachvili, J. N.; Kohonen, M. M. Evaporation and Instabilities of Microscopic Capillary Bridges. *Proc. Natl. Acad. Sci. U.S.A.* **2003,** *100*, 803–808.
(50) Benatov, L.; Wettlaufer, J. S. Abrupt Grain Boundary Melting in Ice. *Phys. Rev. E* **2004,** *70*, 061606.
(51) Xiao, R. F.; Alexander, J. I. D.; Rosenberger, F. Morphological Evolution of Growing-Crystals — A Monte-Carlo Simulation. *Phys. Rev. A* **1988,** *38*, 2447–2456.
(52) Angell, C. A. Insights into Phases of Liquid Water from Study of Its Unusual Glass-Forming Properties. *Science* **2008,** *319*, 582–587.
(53) Banerjee, D.; Bhat, S. N.; Bhat, S. V.; Leporini, D. ESR Evidence for 2 Coexisting Liquid Phases in Deeply Supercooled Bulk Water. *Proc. Natl. Acad. Sci. U.S.A.* **2009,** *106*, 11448–11453.
(54) Donati, C.; Douglas, J. F.; Kob, W.; Plimpton, S. J.; Poole, P. H.; Glotzer, S. C. Stringlike Cooperative Motion in a Supercooled Liquid. *Phys. Rev. Lett.* **1998,** *80*, 2338–2341.
(55) Mader, H. M. The Thermal-Behavior of the Water-Vein System in Polycrystalline Ice. *J. Glaciol.* **1992,** *38*, 359–374.
(56) Nye, J. F. Thermal-Behavior of Glacier and Laboratory Ice. *J. Glaciol.* **1991,** *37*, 401–413.
(57) Guzmán, M. I.; Hildebrandt, L; Colussi, A. J.; Hoffmann, M. R. Cooperative Hydration of Pyruvic Acid in Ice. *J. Am. Chem. Soc.* **2006,** *108*, 10621–10626.
(58) Burgess, K.; Han, J. Fluorescent Indicators for Intracellular pH *Chem. Rev.* 2009, doi: 10.1021/cr900249z.
(59) Salerno, M.; Ajimo, J. J.; Dudley, J. A.; Binzel, K.; Urayama, P. Characterization of Dual-Wavelength Seminaphthofluorescein and Seminapthorhodafluor Dyes for pH Sensing under High Hydrostatic Pressures. *Anal. Biochem.* **2007,** *362*, 258–267.

DOI: 10.1021/jz9000888 | *J. Phys. Chem. Lett.* **2010,** *1*, 374–378